

## EXPERIMENTAL STUDY OF THE RUNUP OF TSUNAMI WAVES ON A SMOOTH SLOPING BEACH

DAVID J. MCGOVERN<sup>1</sup>, IAN CHANDLER<sup>2</sup> AND TIZIANA ROSSETTO<sup>3</sup>,

*1 University College London, U.K., d.mcgovern@ucl.ac.uk*

*2 HR Wallingford, U.K., ian.chandler@hrwallingford.com*

*3 University College London, U.K., t.rossetto@ucl.ac.uk*

### ABSTRACT

A series of large-scale laboratory flume experiments are performed using a pneumatic long-wave generator to simulate tsunami-length trough-led waves. The periods generated are from approximately 6.5 – 37, 40, 72 and 230 s. The runup of these waves is measured on a 1:20 sloping beach. Preliminary results from these tests are presented. The reflections of long waves is discussed. Runup of the 230 s waves is found to be lower than the waves with periods of less than 72 s and previously published data in the literature. Plots of various wave parameters against runup show the strongest positive correlations to be with the crest amplitude and the total potential energy for all wave periods presented. The shorter period data shows a reasonably good fit to available runup relationships, with the longer 40, 72 and 230 s waves showing a poorer fit, suggesting another relationship. Outlines of extensive further work is also given.

**KEYWORDS:** Tsunami, Runup.

### 1 INTRODUCTION

Tsunamis are generated by undersea mega-thrust earthquakes and present a significant natural hazard to adjacent coastlines. The 2004 Indian Ocean Tsunami and 2011 Tohoku Tsunami together caused the loss of approximately 300,000 lives and billions of dollars in economic and infrastructure losses (e.g., Kajitani et al, 2013). The behaviour of tsunami in the nearshore region is not well understood due to the inherent complexities and non-linearity of their interaction with coastlines. There is an urgent need for an improved understanding of the near and onshore behaviour of tsunami and their interaction with coastlines and structures.

Within that need is a specific improvement to the understanding of tsunami runup on coastlines. Runup  $R$  is the vertical height above local static water level of the inland limit of tsunami inundation for a given wave. It is a commonly used parameter in the assessment of tsunami interaction with a shoreline and particularly for risk analysis, planning and insurance. Runup has been the subject of extensive previous research. Carrier and Greenspan, (1958) provide analytical solutions of runup over a smooth impermeable bed. Synolakis (1987) presents analytical solution for solitary wave runup supported by a series of experiments on a smooth beach. Numerous analytical and numerical studies have been conducted using solitary waves (for example, Zelt, 1991 and Borthwick et al., 2006). However, the validity of the solitary wave paradigm was first questioned by the results of Tadepalli and Synolakis (1994) whose results show that maximum runup for a trough-led N-wave was greater than for the equivalent solitary wave. This indicates that wave shape was an important parameter. A thorough treatise by Madsen et al., (2008) suggests that solitary waves fail to adequately model specific characteristics of tsunami. Indeed, Charvet et al., (2013) present experimental evidence that the solitary wave, which is a steep positive elevation, actually results in a conservative estimation of runup when compared to longer elevated waves with shallower steepness but of equivalent amplitude. Their experimental data (collected using an earlier version of the pneumatic long-wave generator applied in this research) also highlights the lack of accurate runup prediction for tsunami waves. This is due to a lack of relevant experimental data, particularly for tsunamis of the general form of N-waves, which are regarded as much more representative of tsunami than the previous simplification of solitary waves (Madsen et al., 2008). Charvet et al., (2013) presents new empirical predictor equations based on a series of trough-led and elevated wave tests in a 45 m long flume. Their data suggests that the potential energy  $E_p$  of the wave should be considered as an influential parameter to runup, along with

traditionally used metrics such as amplitude  $a$  and wavelength  $\lambda$ . (It is important to note that defining the wavelength for solitary waves is particularly subject to the method of defining this parameter.)

Experimental data of long wave interaction with structures and coastlines are relatively rare. This is mainly due to the often-bespoke requirements of reproduction of long wave periods in hydraulics laboratories. Even at model scale, tsunami wavelength often measures hundreds of metres, necessitating very long flumes to accommodate the target characteristics of the wavelength before reflections contaminate the desired free-surface profile. Further, it is not easy to produce both tsunami wavelength and amplitude using traditional piston-type wave making devices. Some success at very small scale with piston paddles in a very large flume has been reported by Schimmels et al., (2014). However, the amplitudes for tsunami-like wave periods upgrade to relatively low values in the prototype, and the scale of the experiments was limited due to the maximum stroke of the piston-type wave maker. Gosberg et al., (2013) describe the successful implementation of a pump methodology to generate tsunami in a closed-circuit flume. There are limitations to the wave heights producible at larger depths by the method, which also limit its scalability to prototype depths in the particular facility described. To produce long waves, we use the HR Wallingford pneumatic long-wave generation system as described in Rossetto et al., (2011). This allows for large amplitude very long waves to be generated through water volume exchange between the generator and the flume. The design and set-up of the current pneumatic generator allows the generation of waves of period  $T \leq 240$  s. Its development is described in Allsop et al., (2014).

This paper presents initial results of an extensive test programme the first phase of which has recently been completed. It should be treated as a ‘work-in-progress’. The paper is organised in the following way. Section 2 describes the experimental set-up for the runup tests. Section 3 presents data to validate the current experimental setup. This includes selected very long period N-wave runup results from an extensive series of long wave experiments. Comparisons are made with the present trough-led N-wave results and relevant published data. Some considerations of the modelling of very long waves in the current facility are also made as well as analysis and discussion of the wave celerity. Finally, a discussion of the sensitivity of runup to various parameters is given and the presented data is compared to available empirical equations. In section 4 the future work that is ongoing in this field within the research project URBANWAVES is highlighted.

## 2 EXPERIMENTAL SET-UP AND DATA ANALYSIS

The long-wave generator is installed at the far end of the 100 m long, 1.8 m wide flume at HR Wallingford, U.K. At the opposite end a 1:20 sloping bathymetry is installed reaching a maximum height of 1 m. This is the nominal position of the shoreline. Runup is recorded on an extended beach from this position adding a further 5 m of slope. Figure 1a presents a schematic diagram of the set-up.

Trough-led N-waves are progressive waves with a leading negative elevation followed by a positive elevation. A large range of wave periods are tested from  $T \approx 6.5 - 240$  s. The latter periods are thought by the authors to be amongst some of the longest wave periods produced in a laboratory to date.  $T$  is defined as the time difference between the start of the trough and the start of the crest,  $T_1$  added to the time difference between the start of the crest and the top of the crest,  $T_2$  multiplied by 2 (Figure 1b). Further, a wide variation of positive amplitudes  $a^+$  and negative amplitudes  $a^-$  are generated along with variations in the length and height of the troughs and crests of the N-waves.

The surface elevation  $\eta$  is recorded for each test at various locations in the offshore (constant depth region of the flume), the nearshore (above the sloping bathymetry) and onshore (extended beach) regions of the flume using 16 resistance-type wave gauges. These gauges are calibrated daily before testing. Runup length  $R_L$  is read from a tape measure on the centreline of the beach with an accuracy of  $\pm 0.005$  m. This is then converted to the runup height  $R = R_L \sin\beta$ , where  $\beta$  = the angle of the slope. Time series velocity profile data is collected at the bathymetry toe using a Nortek ADCP and near the bed towards the beach using a Nortek Vectrino.

Charvet et al., (2013) presents empirical relationships of runup based on the estimation of the potential energy  $E_p$  of the offshore waveform. In linear shallow water conditions the wave profile should not significantly change in the offshore region with time. In such cases  $E_p$  can be expressed as (1):

$$E_p = \int_0^T \frac{1}{2} g \rho \eta(t)^2 C dt \quad (1)$$

Where  $g$  = acceleration due to gravity,  $\rho$  = density of water,  $T$  = instantaneous time and  $C$  = wave celerity.  $C$  is calculated from the temporal correlation of the wave between the probes situated at the bathymetry toe and in the offshore region.

## 3 RUNUP

The first goal of the tests is to validate the current long-wave generator and laboratory set-up. This is achieved by running a series of relatively shorter period (in terms of what the generator can produce) trough-led N-waves and plotting the calculated runup against relevant previously published data. Figure 2 shows the runup normalised with offshore water depth  $R/d$  versus positive amplitude over depth  $a/d$  of selected trough-led N-waves with periods ranging from  $T \approx 6.5$  s - 37 s (plot with ‘□’ symbols). The trend follows that of Charvet et al., (2013)’s N-wave data (‘\*’ symbols,  $T \approx 6.6$  s – 8.8 s) and the solitary wave

data of Synolakis (1987, ‘.’ symbols) closely. The N-waves presented vary in shape; they are not symmetrical in the vertical or horizontal plane and generally exhibit shallower troughs than crests. These waves also have much longer periods so that the majority do not form plunging breakers. The data presented from Charvet et al (2013) is exclusively for breaking N-waves. Neither the data of Charvet et al (2013) nor the current data exhibit the distinct change in relationship of the Synolakis data between breaking (either during runup or backwash) and non-breaking waves. In the current tests, breaking is only recorded for the runup, though regardless the same trend is not seen in the data. The water depth  $d \approx 1$  m is larger in the current tests than in Charvet et al., (2013). However, this is not thought to be an influencing parameter on  $R$ , as shown in correlation plots of  $R$  vs  $d$  (Figure 4, §3.4) with the current data and that presented by Charvet et al., (2013).

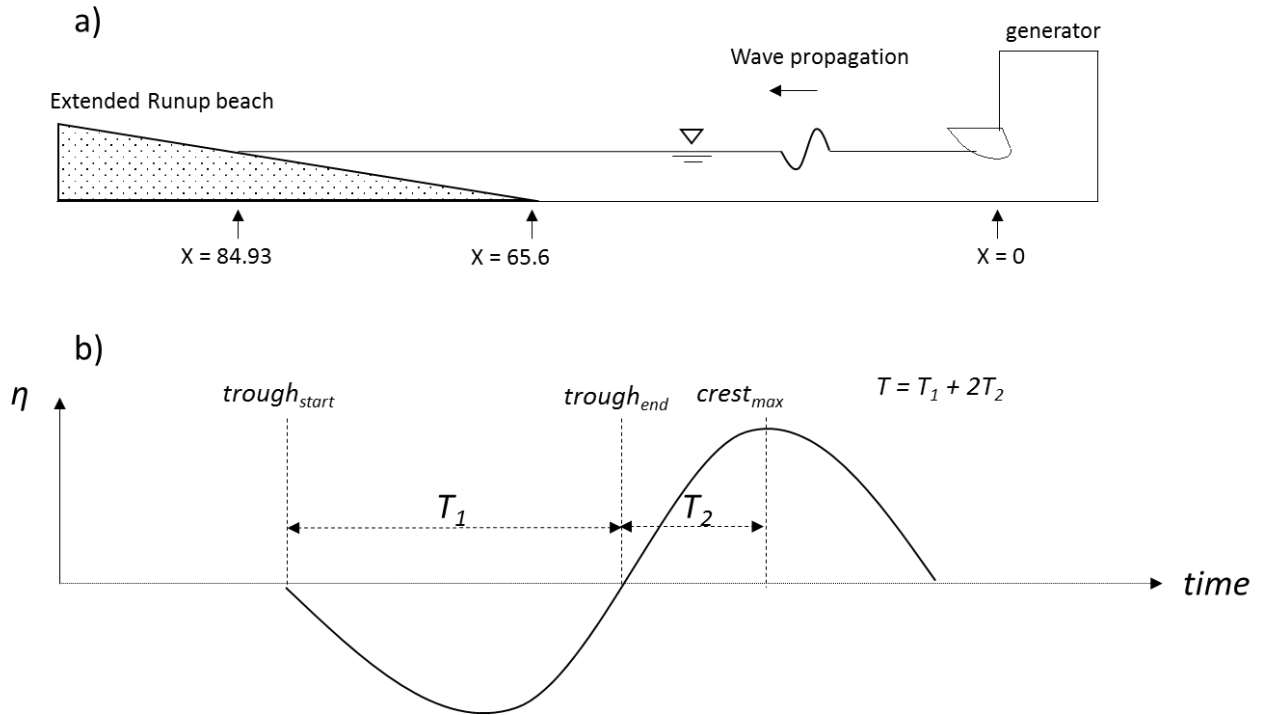


**Figure 1(a).** Schematic diagram of the experimental set-up for the runup tests (not to scale). **Figure 1(b).** Schematic diagram showing the definition of period  $T$  for the trough led N-waves.

### 3.1 Runup of Very Long Waves

Previous data sets focus on solitary waves with periods that when scaled up to prototype are considerably shorter than actual tsunami, such as Synolakis (1987). Charvet et al., (2013) presents trough-led N-wave data that is generally  $T < 10$  s with three tsunami-length waves of  $T \approx 99 - 172$  s model time. For the tsunami-length waves it is difficult to determine what the role of reflections may have had in the smaller flume length in which those experiments were conducted. The aim of the current tests is to extend the experimental data set to waves of tsunami-length at prototype Froude scale of (say) 1:50. Specifically a set of six vertically and horizontally symmetrical N-waves of  $T \approx 40$  s (which at 1:50 scale is a 4.7 minute wave), 80 s (9.4 min), 111 s (13 min), 166 s (19.5 min), 200 s (23.5 min) and 240 s (28.3 min) are generated, allowing the isolation of  $T$  as the varying parameter to  $R$  (see also Chandler et al., 2016). [Two cautionary notes: actual periods varied from the target period in some cases, for example the  $T \approx 80$  and 240 s waves are closer to  $T \approx 72$  and 230 s respectively in reality; and the relationships between wave height and duration do not necessarily abide by the classic definition of an N-wave.]

We present six, ten and seven data points from the symmetrical  $T \approx 40, 72$  and 230 s trough-led N-wave in Figure 2, (‘ $\Delta$ ’ symbols, ‘o’ symbols and ‘down-triangle’ symbols). The data shows good repeatability (mean  $R/d = 0.045, 0.109$  and  $0.205$ , standard deviation  $\sigma = 0.003, 0.005$  and  $0.002$ , mean  $a/d = 0.038, 0.035$  and  $0.059$ ,  $\sigma = 0.002, 0.0003$  and  $0.0012$  for the 230, 72 s and 40 s waves respectively) between each test. The  $T \approx 72$  and 40 s data match the shorter period  $T \approx 6.5 - 37$  s data and that previously published on Figure 2 well.

The  $T \approx 230$  s data is clearly offset to the remaining data on Figure 2. The offset is indicative of a different relationship between  $R$  and  $a$  for longer period waves, and this is also observed for the waves with  $T \approx 111 - 200$ , the data of which are not presented here, but shows a linear relationship of  $R/d$  increasing with  $a/d$  which is at the same offset ratio as the 230 s data. For waves of  $T \leq 72$  the data converge with the shorter period data discussed above, and that of Charvet et al., (2013) and Synolakis (1987). The data implies a change in the influence of  $a$  on  $R$  at some particular or range of  $T$ , and this will be investigated further later in this paper and in-depth in a future publication. Further, and as discussed below, a more comprehensive analysis of the generation of very long waves in the flume is needed to give additional confidence to the above

findings.

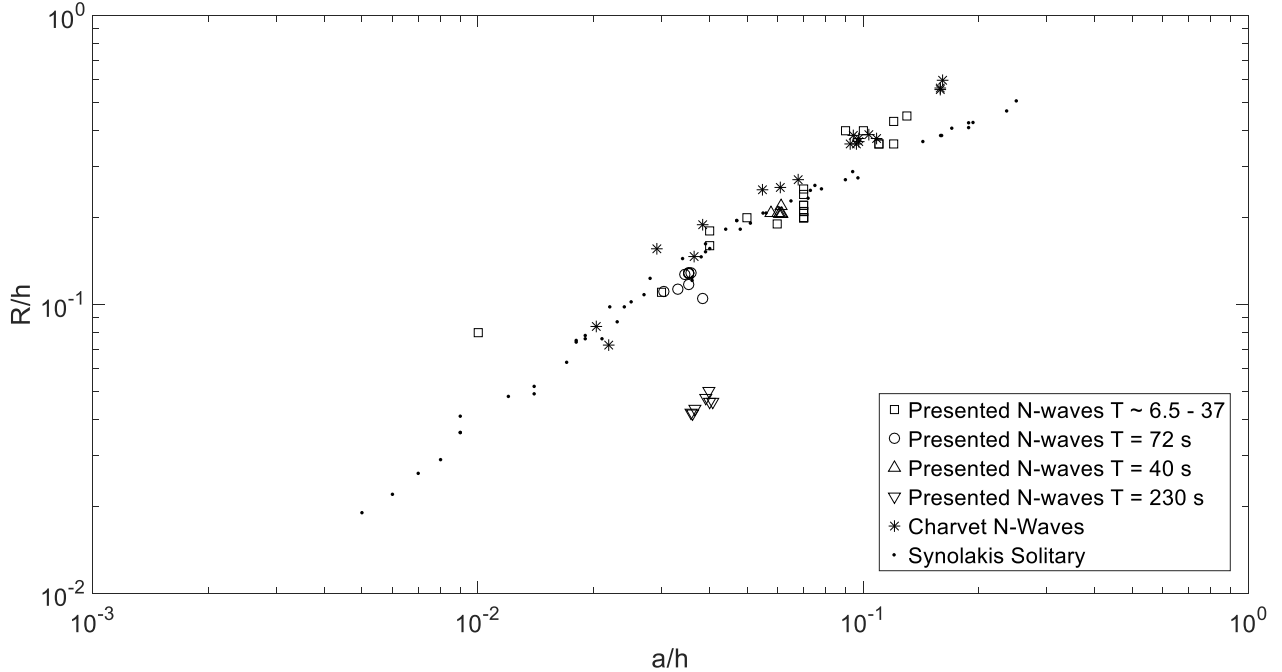


**Figure 2.** Plot of  $R$  and  $a$  normalised with  $d$  for the present trough-led N-waves of periods  $T \sim 6.5 - 37$  s data ( $\square$  symbols),  $T \sim 40$  s data ( $\triangle$  symbols),  $T \sim 72$  s data ( $\circ$  symbols),  $T \sim 230$  s data ( $\nabla$  symbols), and trough-led N-wave data from Charvet et al., (2013,  $*$  symbols) and Synolakis (1987) short period solitary wave data ( $\cdot$  symbols).

### 3.2 Considerations of Very Long Wave Generation

Figure 3a-c presents typical symmetrical 40 s, 72 s and 230 s wave profiles from the wave gauges positioned in the offshore and nearshore regions covering a range of  $X = 7.02 - 83.6$  m. The wave is defined at the gauge nearest to the generator ( $X = 7.02$  m, dashed-dot line Figure 3a-c). The wavelength is calculated as  $\lambda = C \cdot T$ . The mean values of these properties for the six 40 s, ten 72 s and seven 230 s waves are given in Table 1. The definition of the waveform parameters can take place at any point in the offshore region of the flume, before the wave begins to shoal. We choose the gauges near the generator ( $X = 7.02 - 22.02$  m) as these gauges are well away from the shoaling effects of the bathymetry. Further, in the 40 s wave, it is clear that the offshore waveform does not change with  $X$  indicating that the wave is generally behaving as a linear shallow water wave and does not significantly disperse. The absence of significant change in the waveform allows  $C$  to be defined from the temporal correlation of the beginning of the crest between two adjacent wave gauges at  $X = 7.02$  m and  $12.02$  m, and  $T = T_1 + 2T_2$  using the method described in Figure 1. The beginning of the crest is defined as the time instance of the first up-crossing of  $\eta$  above a value of 1% of the measured  $a^+$ . This was used in preference to the down-crossing of the start of the trough or the max crest elevation correlation as it was consistently found to be the most clearly defined of the three wave parts in most of the wave periods tested.

The ability to reproduce prototype conditions in this flume is key to the validity of these tests to prototype conditions. As the  $\lambda$  of the wave is significantly longer than the length of the flume, the effect of reflections on the runup requires consideration. The first reflection is from the start of the trough off the rear of the generator (which is a vertical flat steel panel) and back into the flume. This will increase the apparent depth of the trough recorded in the offshore region. However, from the data this appears not to be significant, likely because the reflection is minimal as most of the water is moved into and upwards within the generator and relatively slowly for these long period waves. The second reflection point is from the start of the first shoreward motion of the water from the generator that occurs after the base of the trough has been generated. This, upon reaching some position on the bathymetry (the reflection point) will generate a reflection that will travel back to the rear of the generator and eventually be reflected once more into the flume.

The  $T \approx 40$  s waveform as recorded at the first four wave gauges shows no destructive interference from the natural reflection of the trough and therefore the "false" re-reflection. At gauge positions  $X = 7.02, 12.02, 17.02$  and  $22.02$  m the whole wave profile passes the measurement point before the natural reflection will return, as calculated with the experimentally derived  $C$ . Its wavelength,  $\sim 130$  m is still longer than the flume but the re-reflection does not interfere with the target waveform before the full crest has passed the gauges near the generator and, therefore, all gauges in the flume.

The  $T \approx 72$  s wave shows distinct destructive interference with the wave crests recorded at the wave gauges at  $X = 7.02, 12.02, 17.02$  and  $22.02$  m. The natural reflection of the base of the trough from the bathymetry ought to conservatively return

to these gauges at  $\sim 124$  s, 123 s, 122 s and 121 s respectively in absolute time (time  $t$  as given on the x-axes of Figure 3a-c) after the data collection begins. The toe of the bathymetry ( $X = 65.6$  m) can be used as a conservative reflection point although the majority of the reflection will probably from further up the slope in shallower water. The destructive effect increases with time as the trough passes back towards the generator. Because it reaches the gauges sequentially earlier on the rise of the crest with increasing distance  $X$  from the generator, the crests are reduced further with increasing  $X$ . The re-reflection will then begin to affect the wave traces at a particular  $X$  position  $\sim 39$  s after the base of the trough has passed that point. This for all the wave gauge traces is  $\sim 7$  s after the crest has passed and appears to cause a slight steepening of the rear of the crest. Further, the remainder of the re-reflected trough, which is generated between  $t \sim 90 - 110$  s is interfering with the traces again at  $t \sim 129 - 149$  s which may explain the increased size of the second trough in the traces. The wave gauge at  $X = 47.02$  m shows a reduced crest and lengthened trough. This can be explained by the natural trough reflection, which at this position takes only  $\sim 11$  s to return to the gauge. Hence the trough will destructively interfere with the crest up to  $t \sim 141$  s. This has the effect of lengthening the trough and shortening the crest. At  $X = 65.6$  the natural trough and crest reflection is (conservatively) essentially immediate and so the interference is likely only constructive. Hence the large amplitude, which is possibly enlarged further by natural shoaling as the wave begins to move into smaller depths.

Additionally the re-reflected initial crest reflection is constructively interfering with the second crest thus increasing its height as also observed. These reflections affect the waveform well after the top of the crest and are, therefore, not a significant factor in the proper generation of the wave. The exception is for the wave gauge at  $X = 47.02$  m, where the false reflection will return at  $t \sim 145$  s, which coincides with the wave crest at this point, likely due to the stretching of the trough by the destructive interference of the natural trough reflection. This explains why the crest is significantly reduced in height, as well as the appearance of shorter frequency fluctuations on the crest and thereafter which could be attributed to linear dispersion of the reflected wave. Further analysis is required to determine the interaction of the free and reflected waves with certainty.

The typical  $T \approx 230$  s (Figure 3c) waveform does not change in the offshore or nearshore region, indicating that the wave is generally behaving as a shallow water wave and does not significantly disperse. The  $T$  and  $C$  are estimated from the temporal correlation of the beginning of the trough, defined as the time instance of the first down-crossing of  $\eta$  below a value of 1% of the measured  $a$ . There is a notable but relatively minor shorter period ( $\sim 22$  s) signal superimposed on the wave trace, but its amplitude does not significantly affect the target wave profile and properties. This period is likely due to either, or a combination of, the resonant frequency within the flume (estimated at 44 - 49 s, of which the short period slosh coincides with the 2<sup>nd</sup> harmonic) for this particular water depth and bathymetry configuration, and fluctuations in the inertia of the free surface within the generator as the wave is generated. Its presence, however, prevents the temporal correlation of the wave between the two gauges by using the arrival of the peak or any other part of the wave other than the trough. This superimposed signal is not observed on waves with  $T \leq 111$  s.

As the  $\lambda$  of the  $T \approx 230$  s waves is  $\sim$  nine times the length of the offshore flume length, the validity of its behaviour in the flume to prototype requires thorough investigation. For the  $T \approx 230$  s waves the reflected trough at the experimentally defined  $C$  is calculated to return  $\sim 53$  s after it first occurs at that position. In Figure 3c this reflection ought to be present in the wave trace at  $t \sim 240$  s coinciding with the peak of the wave. The trace in Figure 3c does not obviously show significant destructive interference. It is possible that the reflected trough follows the generation of the peak down the flume, reducing the height of the peak at all positions. However, this does not seem likely as the shape and symmetry of the wave does not change with  $X$ . An alternative hypothesis is that the reflections present in the test space are corrected by the generator. For instance, by achieving a target wave profile at a particular wave gauge position, the generator compensates for the reflected waves through adjustments in the valve angle  $\theta$  time series input command (see Allsop et al., 2014 and Rossetto et al., 2013 for further details of the generators operational procedure). As the set-up is novel, the commissioning was not done with the aid of a  $\theta(t) \rightarrow$  flume free-surface  $\eta(X, t)$  transfer-function, as would be the case with traditional wave paddle drive computer. It is instead done with an iterative methodology where the  $\theta(t)$  is modified incrementally to achieve the target  $\eta(X, t)$ . Further tests and analysis are required to establish the water flow in the flume over time, the absorption effects if any of the generator, and whether the 230 s wave and other longer waves produced in the test programme are scalable to prototypes (see also Chandler et al., 2016).

**Table 1. The parameters and standard deviations of the three N-wave periods presented.**

Wave	$T$ [s]	$T(\sigma)$ [s]	$a^+$ [m]	$a^+(\sigma)$ [m]	$C$ [m/s]	$C(\sigma)$ [m/s]	$\lambda$ [m]	$\lambda(\sigma)$ [m]
40 s N-wave	39.1	0.2	0.06	0.015	4.5	0.16	176	6.7
72 s N-wave	72.1	2.1	0.035	0.002	3.5	0.53	251.7	33.2
230 s N-wave	230	7.8	0.038	0.0017	2.43	0.097	559	36

### 3.3 Estimation of Wave Celerity

From Table 1 it is clear that the temporal correlation methods described in §3.2 are reasonably consistent. The values for the  $T \approx 40$  and 72 s waves ( $4.5 \text{ m s}^{-1}$  and  $3.5 \text{ m s}^{-1}$  respectively) is faster than shallow water theory predicts ( $\approx 3.13 \text{ m s}^{-1}$ ) by approximately 40.6% and 9.4% respectively. This suggests that those waves are not in the linear regime, as discussed in

Charvet, (2012). The same is found for the shorter period waves of  $T \approx 6.5 - 37$  s, in which the experimentally derived celerity is generally slightly higher than shallow theory predicts (ranging from -10%  $\sim$  +60%). The offshore velocity profile is measured using a Nortek ADCP, while nearer the shoreline point velocity time-series is measured using a Nortek Vectrino ADV. For a long shallow water wave the water particle orbital motion would normally be highly elliptical becoming flatter towards the bed. Real-time observations of the ADCP profile data show nominally 2D velocity; there is negligible vertical flow, suggesting that the particle motion is indeed near-horizontal. These data will be analysed fully in a future publication.

The estimation of  $C$  from the temporal correlation of the waveform between wave gauges is a source of uncertainty for the  $T \approx 40, 72$  and  $230$  s waves. Changes to its value will affect the estimation of  $E_p$ . The determination of  $C$  from the experimental data remains a source of uncertainty and requires further analysis in a future publication. For the  $T \approx 230$  s waves the slower celerity raises various questions of the behaviour of wave that is produced by the generator and requires further analysis before any robust conclusions can be drawn.

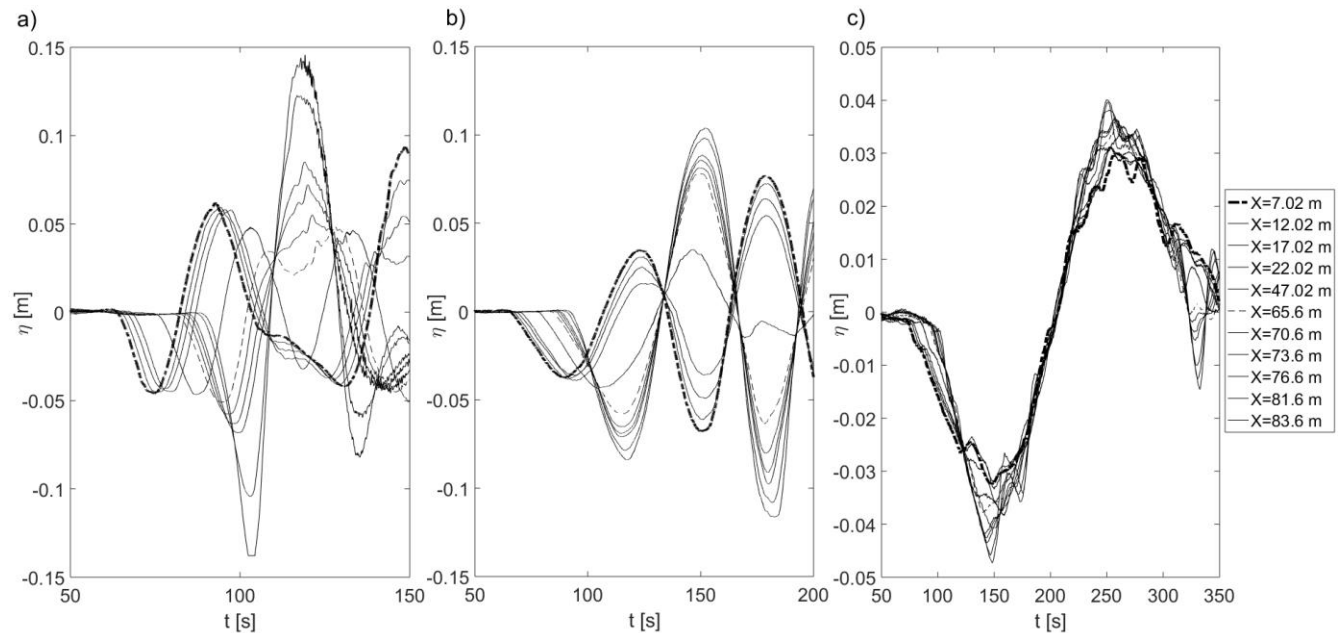


**Figure 3a-c.** Time series free-surface elevation  $\eta$  for typical  $T \approx 40, 72$  and  $230$  s waves for all gauges from  $X = 7.02 - 83.6$  m as a function of  $t$ , where  $t =$  time in s. The wave gauges at  $X = 7.02$  m is highlighted as a dot-dashed line and  $X = 65.6$  m as a thick dashed line. In Figure 3a, the waveform does not significantly change in the offshore or nearshore regions. In Figure 3b, the waveform experiences destructive interference from the natural reflection of the trough. In Figure 3c the waveform does not significantly change in the offshore or nearshore regions.

### 3.4 Correlations between Runup and Characteristics of the Waveform

To determine the sensitivity of  $R$  with the wave characteristics the runup is plot as a function of  $a^+$ ,  $a^-$ , trough and crest length,  $\lambda$ ,  $E_p^+$ ,  $E_p^-$ ,  $E_p$  and  $d$  for the  $T \approx 6.5 - 37$  s data (Figure 4). The data is divided into breaking waves ('o' symbols) and non-breaking waves ('+' symbols). The definition of breaking was applied to those waves whose crest broke during runup as observed on video recordings. The results show a correlation in all plots except  $d$ . This is similar to the findings of Charvet et al., (2013) for their  $T < 10$  s waves, and suggests that wave  $a$  and  $E_p$  (which in the current data appear to show the strongest correlations) are the primary influencing parameters on runup. The exception is for  $\lambda$ , which in the current data shows an, albeit fairly weak, positive correlation whereas Charvet et al., (2013)'s data shows no correlation with  $\lambda$ . The reason given is that in their data, runup has a weaker and negative correlation with trough length and a stronger and positive correlation with crest length. The current data exhibit a relatively similar positive correlation with both trough and crest length. Thus overall wavelength is influenced in the same way by both parameters, unlike in the Charvet et al., (2013) data. The crests of the presented waves are generally larger than the troughs and furthermore, the variation in size and length of the troughs for the presented waves is quite small while being much larger for the crests. The very strong positive correlation in crest amplitude indicates that it is likely the main governing parameter for this particular set of waves. Indeed the much larger values of  $E_p^+$  also indicate that the crest size and length is dominant over the trough size and length for these particular tests. Breaking waves show a generally higher  $R$  likely due to their larger steepness.

In Figure 4 there is an indication of a potential asymptotic limit to  $R$  with  $E_p$ . This limit may well be related to the capacity of the generator to increase the energy of a given wave period (in other words, the largest combination of  $a^+$  for a given  $T$ ), rather than a natural asymptote. This will be analysed with the full data set in a future publication.

The same correlation plot for the  $T \approx 40$  s ('o' symbols) 72 s ('+' symbols) data are given in Figure 5. Here there is a

correlation with all the parameters except for  $d$  and  $E_p^-$ . These waves are nominally symmetrical in length and height and have only relatively small changes to the amplitude and wavelength. Again,  $a^+$  and  $E_p^+$  appear the dominant parameters.  $a^-$  has a weaker positive correlation and appears less influential than  $a^+$ .  $\lambda$  shows no correlation with  $R$  for the  $T \approx 40$  s waves. Crest and trough length show weakly negative correlations with  $R$  for the 72 s N-waves and the correlation of  $\lambda$  matches these quite well as would be expected for symmetrical waves.

With the limited data presented, the following hypothesis can be considered as to why the longer  $T \approx 72$  s waves exhibit a marginally lower runup. The variation in  $\lambda$  of the  $T \approx 72$  s waves, which are due to small changes in the antecedent flume conditions and experimental variability, allow some analysis of the influence of  $\lambda$ . The longer  $T \approx 72$  s have a generally slightly higher  $a$  than the shorter  $T \approx 72$  s waves, indicating that  $\lambda$  (or perhaps the steepness  $a/\lambda$ ) may play some influence. This is perhaps due to the shoaling characteristics of longer waves and will be discussed further in the context of the  $T \approx 230$  s waves.

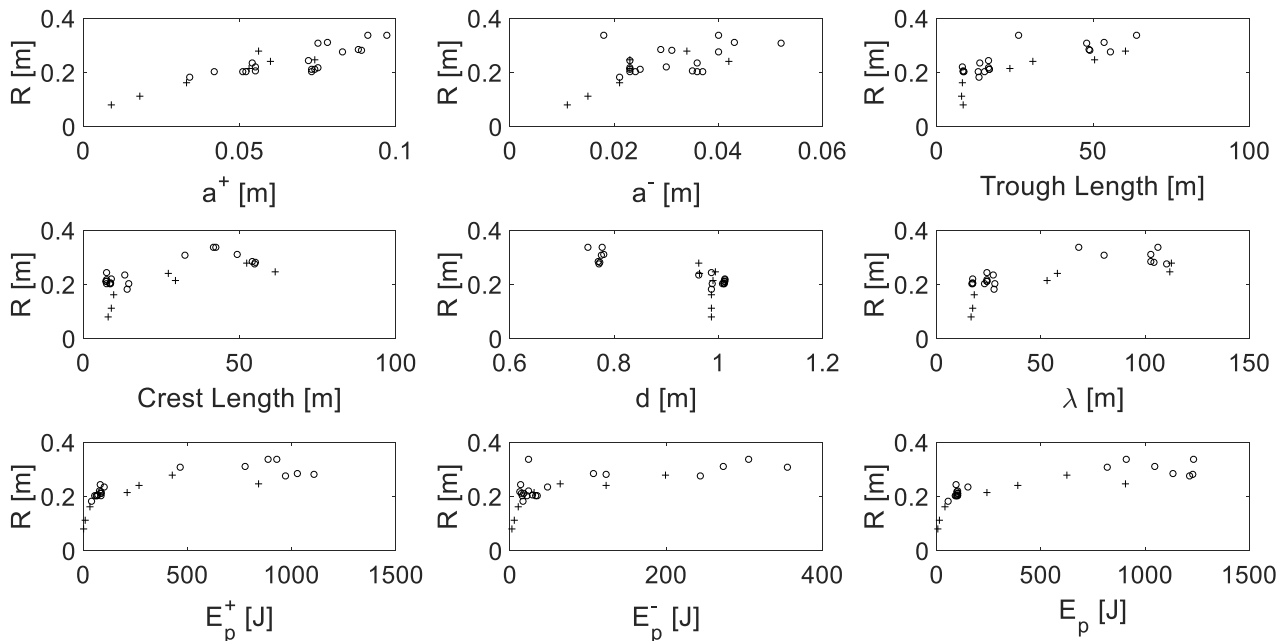


**Figure 4. A selection of correlation plots of the  $T \approx 6.5 - 37$  s trough-led N-waves (non-breaking ‘+’ symbols and breaking with ‘o’ symbols). Correlations are present for all parameters except  $d$ .**

The same correlation plots for the  $T \approx 230$  s data are given in Figure 6. Here there is a correlation with all the parameters except for  $\lambda$ , crest and trough length. These waves are nominally symmetrical in length and height and have only relatively small changes to the amplitude and wavelength (their effective steepness is nominally the same). Again,  $a^+$  and  $E_p^+$  appear the dominant parameters.  $a^-$  has a weaker positive correlation and appears less influential even though it is slightly larger than  $a^+$ . While  $d$  appears to exhibit a negative correlation the variation in  $d$  is negligible for these tests and thus this may not be a causal relationship.  $\lambda$  does not exhibit a correlation suggesting that for very long symmetrical waves, the trough and crest act to cancel each other out, leaving amplitude as the dominant influencing parameter.

Regarding the offset of the runup for these  $T \approx 230$  s waves against the other data (Figure 2), it is interesting to observe that the recorded runup is very similar to the offshore wave amplitude for the  $T \approx 230$  s waves where as for the  $T \approx 6.5 - 37$  s waves the runup is significantly higher. Analysis of nearshore and onshore wave gauges for the  $T \approx 230$  s waves show the shoaling to be negligible (Figure 3), indicating that the offshore amplitude is essentially the same as the onshore amplitude. This suggests of a different regime of shoreline impingement for these longer waves. Shorter waves will exhibit some fluid acceleration from breaking and near-breaking (surging) on a beach leading to a larger  $R$ . This is opposed to the slow rise in water level induced by the longer wave inundation.

This hypothesis, which also relates to the longer  $T \approx 72$  s waves described above can be developed by considering the following. The very long waves presented possess relatively large energy with relatively slow particle velocity and phase speed, compared to the shorter waves. For waves to shoal significantly they must respond to increasing bed friction in the progressively shallower nearshore reducing their celerity enough to allow the rear of the wave to catch up with the front, thereby growing in height and reducing in wavelength. For these very long waves the offshore celerity is low meaning the reduction of wavelength is slower and takes place over a very long length. It is further limited by the offshore water depth and the length of the flume. Nearshore the relatively high energy and slow celerity reduces the friction loss of both these components. Thus for very long waves in the current flume shoaling is minimal, meaning the offshore wave amplitude remains nominally constant throughout the flume. Hence, the recorded runup is necessarily similar to the offshore amplitude. Shorter

waves will also exhibit more fluid acceleration when surging onto the beach leading to a larger  $R$ . For the  $T \approx 72$  s waves, the above is further weighted by the fact that  $E_p$  is larger for the longer steeper waves but  $R$  is less. This will be addressed in more detail, including its relevance to prototype conditions, and the period threshold between very long wave inundation and shorter, more significantly shoaling wave inundation with additional data of  $T \approx 40 - 230$  s in an upcoming publication.

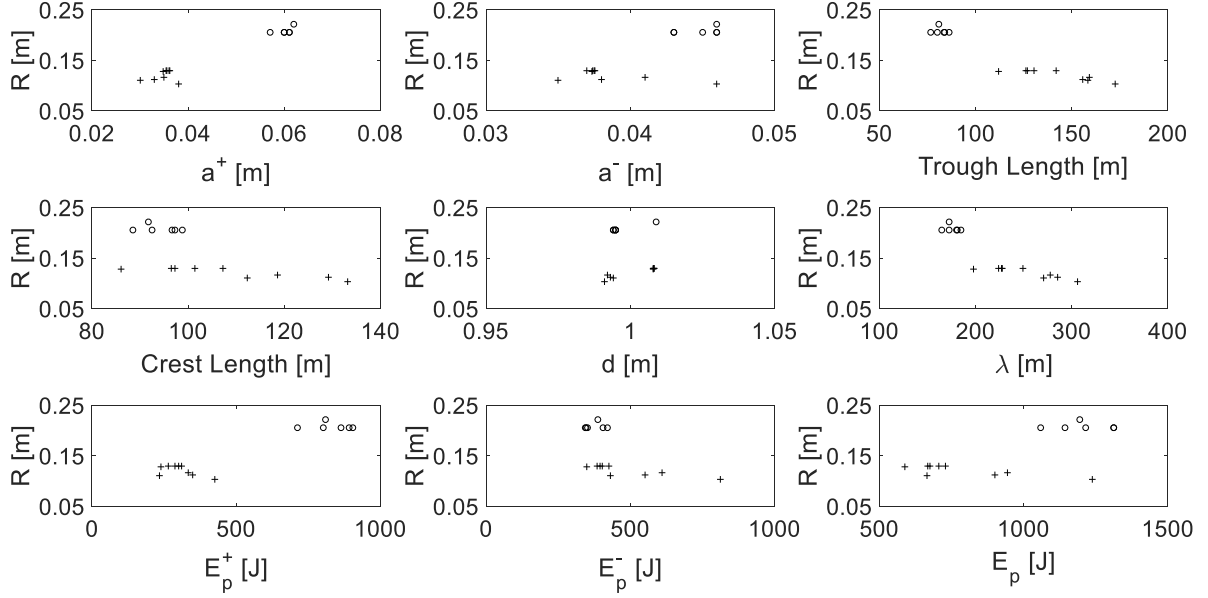


**Figure 5. A selection of correlation plots of the  $T \approx 40$  (‘o’ symbols) and 72 s (‘+’ symbols) trough-led N-waves. Correlations are present for all parameters except for  $d$ . Waves of this length are all non-breaking.**

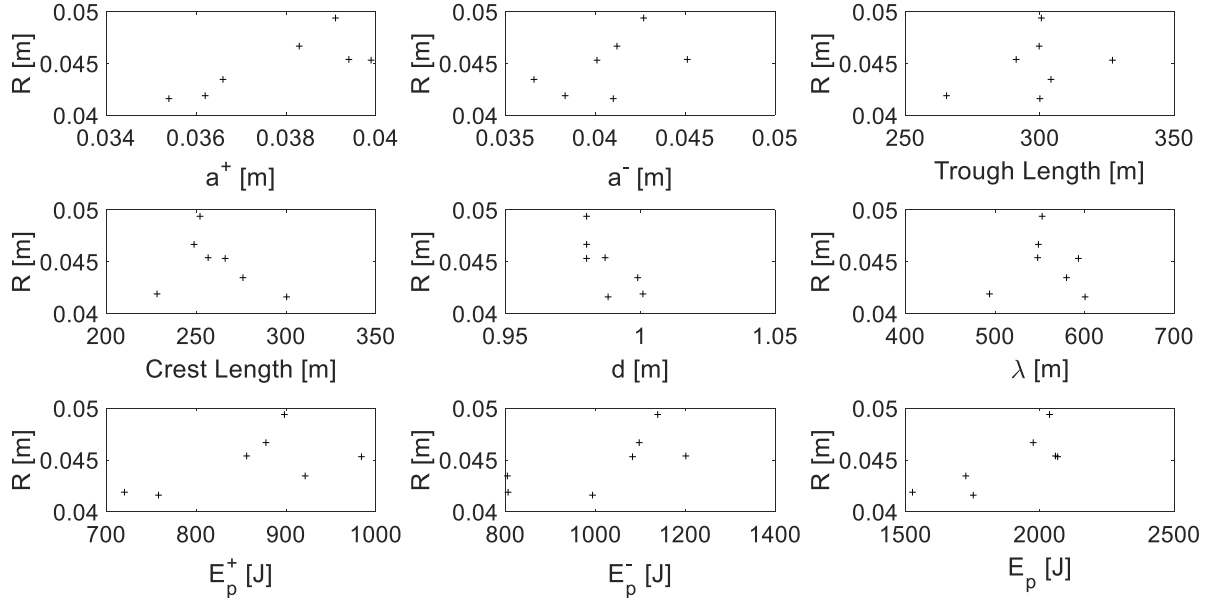


**Figure 6. A selection of correlation plots of the  $T \approx 230$  s trough-led N-waves. Correlations are present for all parameters except  $d$  and  $\lambda$ .**

### 3.5 Comparison with Previous Runup Relationships

Charvet et al., (2013) presents a selection of empirical predictor equations to estimate  $R$  for trough-led N-waves based on the dimensional analysis of the correlations of  $R$  with parameters characterizing the wave. These parameters include  $a$ ,  $\lambda$ ,  $E_p$ ,  $T$ . The waves are categorised using the parameter  $T_b$ , where  $T_b$  = the time taken for a given wave to travel the length of the beach  $l_b$ . This is estimated from (2).

$$T_b = \int_0^{l_b} \frac{dx}{\sqrt{gh\left(1-\frac{x}{l_b}\right)}} = \frac{2l_b}{\sqrt{gh}} \quad (2)$$

The average value of  $T_b$  in the current tests is  $\approx 3.2$  s, which is significantly lower than that of Charvet et al., (2013) who deploy a significantly longer beach length,  $T_b \approx 11$  s. They present the following predictor equations for ‘long waves’ where  $T/T_b < 1$  (3), ‘very long waves’ where  $T/T_b > 1$  (4) and a general equation for N-waves (5).

$$\frac{R}{d} = 5.75 \left( \frac{E_p^+}{\rho g a \lambda d^2} \right)^{0.4} \quad (3)$$

$$\frac{R}{a^-} = 0.27 \left( \frac{E_p^-}{\rho g a \lambda d^2} \right) \quad (4)$$

$$\frac{R}{a^-} = 10.7 \left( \frac{E_p^+}{\rho g a \lambda (a^-)^2} \right)^{0.4} \quad (5)$$

Figure 7(a) shows the predicted runup  $R_p$  as given by equation (3), plotted against the recorded  $R$  values for the  $T \approx 6.5 - 37$  s waves. Equation (3) gives the best results with a favourably conservative overestimation of the actual recorded  $R$  for most waves. Interestingly, this equation is based on shorter period data than most of that of which it is plot against yet still gives reasonable estimates of the runup. The implication is, that with some refinement, equation (3) may be reasonably robust for shorter period N-waves. However, as below, this does not include longer period N-waves and the threshold of maximum period to which (3) could apply will require analysis of the  $T \approx 40$  and  $72$  s data that will be presented in a future publication. It also suggests that the use of the dimensionless variable  $T/T_b$  may not be the most relevant.

Equations (4) and (5) perform very poorly, giving gross underestimations of runup (the data of which is not shown here). Equations (4) and (5) are based on limited experimental data (three waves  $T \approx 99 - 172$  s, Charvet et al., 2013), and as such their validity to longer period waves is uncertain. The use of  $E_p^-$  and  $a^-$  in (4) and (5) may also be a source of error in the prediction as the correlation plots in Figures 4 and 5 suggest that  $E_p^+$  and  $a^+$  are the most influential parameters for the runup of these longer period waves.

Figure 7(b) shows the predicted  $R_p$  from equation (3) plot with the recorded  $R$  values for the  $T \approx 40, 72$  and  $230$  s waves. As with the  $T \approx 6.5 - 37$  s waves, equations (4) and (5) perform very poorly, greatly underestimating the runup (data not shown here). Equation (3) gives values of  $R_p$  that are significantly higher than the recorded data. For the  $T \approx 230$  s wave data, this is expected when considering the lower  $R/a$  ratio for these very long waves, as discussed in §3.4. For the  $T \approx 40$  and  $72$  s data this might be expected with the hypothesis of longer wave impingement expressed in §3.4, but this requires further analysis. In the first instance, however, the implication is that for very long waves (3) requires some refinement.

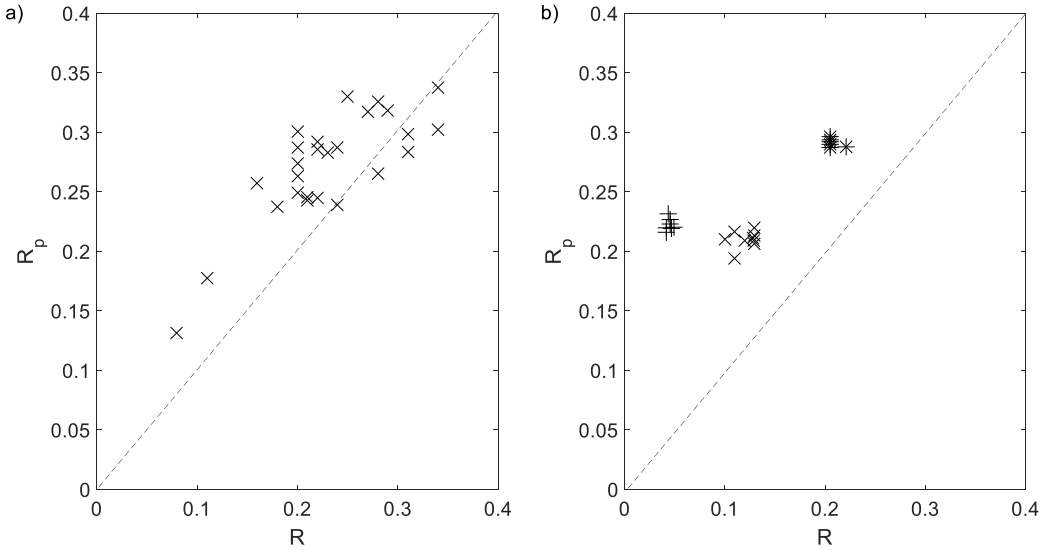


**Figure 7a-b.** Plot of the predicted runup  $R_p$  using equation (3) against recorded runup  $R$  for the  $T \approx 6.5 - 37$  s (Figure 6a) and for the  $T \approx 40, 72$  and  $230$  s data (Figure 6b, ‘\*’ symbols, ‘X’ symbols and ‘+’ symbols respectively).

#### 4 INITIAL CONCLUSIONS AND FURTHER WORK

This paper presents a small selection of tests from an extensive experimental program the runup of tsunami on a sloping beach. This paper specifically concentrates on the runup measurements for a set of very long period ( $\approx 40, 72$  and  $230$ s) trough-led N-waves. These are compared with trough-led N-waves of period  $\approx 6.5 - 37$  s and the existing data available in the literature for shorter period N-waves and solitary waves. For the very long waves, the runup is found to be similar to the shorter waves.

Discussion of the validity of the scaled tsunami N-waves in the test facility shows that there appears to be minimal

reflection issues for waves with significantly longer lengths than that of the facility ( $T \approx 40$  and  $72$  s waves). It is shown that reflections are not detectable in the wave trace until after the crest has passed, allowing the wave to impinge on the shoreline normally. It is also stated that further analysis is required to confirm and quantify the effect of reflections and the relevance of the very long waves generated (in this case the  $T \approx 230$  s) to prototype conditions.

Correlation plots of the key parameters that describe the waveform versus runup show that the crest amplitude and the potential energy are the most significant.

Comparison of the recorded N-wave wave runup data with empirical equations available in the literature show the predictions may still require some improvement.

The data presented here is a limited selection of an extensive data set covering a comprehensive range of N-waves and elevated (solitary-like) waves from periods of approximately  $6.5 - 240$  s. Along with varying the period, the shape of the waves is systematically varied too. An upcoming publication will address the complete data set for very long N-wave and elevated wave runup on smooth and roughened beaches, with the overall aim being the generation of refined and validated empirical predictor equations. The data will then be extended to different slopes and scenarios using numerical tools.

In addition to the runup parameter, the experimental campaign also investigates the interaction of tsunami waves with coastal defence structures. The body force, pressure, water level, overtopping and velocity are recorded on two vertical walls of different heights for a very wide range of wave period and shape. These results will be presented in a future publication along with an in depth analysis including the presentation of predictive formulae.

## ACKNOWLEDGEMENT

This work is fully funded by the URBAN WAVES ERC Starting Grant: 336084. The experiments use the 2<sup>nd</sup> generation Tsunami Simulator developed and constructed by HR Wallingford and operated onsite at HR Wallingford. The input of other researchers to these experiments is gratefully acknowledged. In no specific order: Prof. William Allsop of HR Wallingford, Prof. Ian Eames, Dr Christian Klettner, Dr Tristan Robinson, Dr Andrew Foster, Dr Crescenzo Petrone and Mr Oliver Cook, all Department of Civil, Environmental and Geomatic Engineering, University College London, Mr Ignacio Barranco Granged of the Department of Civil and Environmental Engineering, National University of Singapore and Dr Ingrid Charvet of Risk Management Solutions.

## REFERENCES

- Allsop, W., Chandler, I., and Zaccaria, M., 2014. Improvements in the Physical Modelling of Tsunamis and their Effects. *Proceeding of the 5th International Conference on Application of Physical Modelling to Port and Coastal Protection, Coastlab14*, Varna, Bulgaria, 29 Sept – 2nd Oct.
- Borthwick, A. G. L., Ford, M., Weston, B. P., Taylor, P. H., Stansby, P. K., 2006. Solitary wave transformation, breaking and runup at a beach. *Maritime Engineering*, 159 (MA3), 97-105.
- Carrier, G. F., and Greenspan, H. P., 1958. Water waves of finite amplitude on a sloping beach. *Journal of Fluid Mechanics*, 17, 97 – 110.
- Chandler, I., Allsop, W., Barranco, I. and McGovern, D. J., 2016. Understanding wave generation in pneumatic tsunami simulators, *Proceeding of the 6th International Conference on Application of Physical Modelling to Port and Coastal Protection, Coastlab16*, Ottawa, Canada, 10-13 May.
- Charvet, I., 2012. Experimental modelling of long elevated and depressed waves using a new pneumatic wave generator. PhD thesis.
- Charvet, I., Eames, I., and Rossetto, T., 2013. New tsunami runup relationships based on long wave experiments. *Ocean Modelling*, 69, 79-92.
- Goseberg, N., Wurpts, A., and Schlurmann, T., 2013. Laboratory-scale generation of tsunami and long waves. *Coastal Engineering*, 79, 57-74.
- Kajitani Y., Chang, S. E., and Tatano, H., 2013. Economic impacts of the 2011 Tohoku-Oki earthquake and tsunami. *Earthquake Spectra*, 29, S1, 457-478.
- Madsen, P. A., Fuhrman, D. R., and Schäffer, H. A., 2008. On the solitary wave paradigm for tsunamis. *Journal of Geophysical Research*. 113, C12012, 1-22.
- Rossetto, T., Allsop, W., Charvet, I., and Robinson, D. I., 2011. Physical modelling of tsunami using a new pneumatic wave generator. *Coastal Engineering*, 58, 517-527.
- Schimmels, S., Sriram, V., Didenkulova, I., and Fernandez, H., 2014. On the generation of tsunami in a large scale wave flume. *Coastal Engineering Proceedings*, 1(34), currents. 14.
- Synolakis, C. E., 1987. The Runup of Solitary Waves. *Journal of Fluid Mechanics*, 185, 523-545.
- Tadepalli, S., Synolakis, C. E., 1994. The run-up of N-waves on sloping beaches. *Mathematical and Physical Sciences*. 445, (1923), 99-112.
- Zelt, J. A., 1991. The run-up of nonbreaking and breaking solitary waves. *Coastal Engineering*, 15 (205), 246.